

Endoplasmic Reticulum-Localized Iridium(III) Complexes as Efficient Photodynamic Therapy Agents via Protein Modifications

Jung Seung Nam,^{†,||} Myeong-Gyun Kang,^{†,||} Juhye Kang,^{†,||} Sun-Young Park,^{‡,||} Shin Jung C. Lee,[†] Hyun-Tak Kim,[†] Jeong Kon Seo,[§] Oh-Hoon Kwon,^{†,‡} Mi Hee Lim,^{*,†} Hyun-Woo Rhee,^{*,†} and Tae-Hyuk Kwon^{*,†}

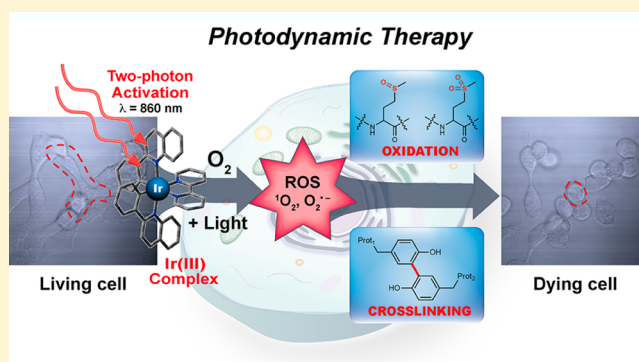
[†]Department of Chemistry, Ulsan National Institute of Science and Technology (UNIST), Ulsan 44919, Republic of Korea

[‡]Center for Soft and Living Matter, Institute for Basic Science (IBS), Ulsan 44919, Republic of Korea

[§]UNIST Central Research Facility, Ulsan National Institute of Science and Technology (UNIST), Ulsan 44919, Republic of Korea

Supporting Information

ABSTRACT: Protein inactivation by reactive oxygen species (ROS) such as singlet oxygen ($^1\text{O}_2$) and superoxide radical ($\text{O}_2^{\bullet-}$) is considered to trigger cell death pathways associated with protein dysfunction; however, the detailed mechanisms and direct involvement in photodynamic therapy (PDT) have not been revealed. Herein, we report Ir(III) complexes designed for ROS generation through a rational strategy to investigate protein modifications by ROS. The Ir(III) complexes are effective as PDT agents at low concentrations with low-energy irradiation ($\leq 1 \text{ J cm}^{-2}$) because of the relatively high $^1\text{O}_2$ quantum yield (> 0.78), even with two-photon activation. Furthermore, two types of protein modifications (protein oxidation and photo-cross-linking) involved in PDT were characterized by mass spectrometry. These modifications were generated primarily in the endoplasmic reticulum and mitochondria, producing a significant effect for cancer cell death. Consequently, we present a plausible biologically applicable PDT modality that utilizes rationally designed photoactivatable Ir(III) complexes.



INTRODUCTION

Photodynamic therapy (PDT) has been successfully used to treat skin cancer by illuminating photosensitizers for over 100 years.¹ Because photosensitizers generate toxic reactive oxygen species (ROS) spatiotemporally by light activation in the treated spaces, PDT has also been applied to many internal cancers.² The most commercialized PDT drug is based on a hematoporphyrin derivative (HPD)³ that generates ROS, leading to tumor cell death. However, limitations of HPD include inefficient light penetration in tissue, poor ROS generation under low dioxygen (O_2) concentrations in physiological conditions of cancer cells,⁴ a low molar absorption coefficient ($1170 \text{ M}^{-1} \text{ cm}^{-1}$)⁵ requiring high treatment doses and longer light exposure time, and side effects including immune response.⁶ Organometallic complexes based on ruthenium (Ru) and platinum (Pt) have been developed to cover such limitations. However, Pt(II) complexes utilize labile ligands for cancer therapy, inducing side effects at unintended sites.⁷ In turn, the poor cell membrane penetration of Ru(II) complexes results in long cell permeation times and relatively high concentration requirements (ca. $40 \mu\text{M}$) for imaging.⁸ The low quantum yields for phosphorescence ($\Phi_p = 0.03\text{--}0.1$) and singlet oxygen ($^1\text{O}_2$) ($\Phi_s = 0.1\text{--}0.5$) in aqueous systems also hinder image-

guided PDT systems.⁹ Subsequent advances in photosensitizer technology have not adequately addressed issues of collateral protein damage, side effects, and cellular substrate reactions effected by ROS.

Herein, we report an effectively developed design strategy for PDT agents based on Ir(III) complexes by controlling their energy levels to achieve marked ROS generation.¹⁰ Ir(III) complexes offer multiple advantages, including (i) simple color tuning, (ii) energy-level control, (iii) long lifetime (microsecond) permitting signal discrimination from protein autofluorescence, and (iv) ROS generation under hypoxia conditions via electron (type I) or energy transfer (type II).¹¹ Furthermore, Ir(III) complexes exert higher anticancer activity against over 60 cancer cell lines than the U.S. Food and Drug Administration-approved drugs, oxaliplatin and cisplatin.¹²

To date, no in-depth research for ROS property enhancement via a molecular design strategy has been performed. Accordingly, we designed four Ir(III) complexes (TlIr1–4; Figure 1a) that exhibit different energy levels as well as distinct Φ_p and Φ_s . Our Ir(III) complexes exhibited two-photon absorption, followed by ROS generation, which might represent

Received: May 23, 2016

Published: August 5, 2016

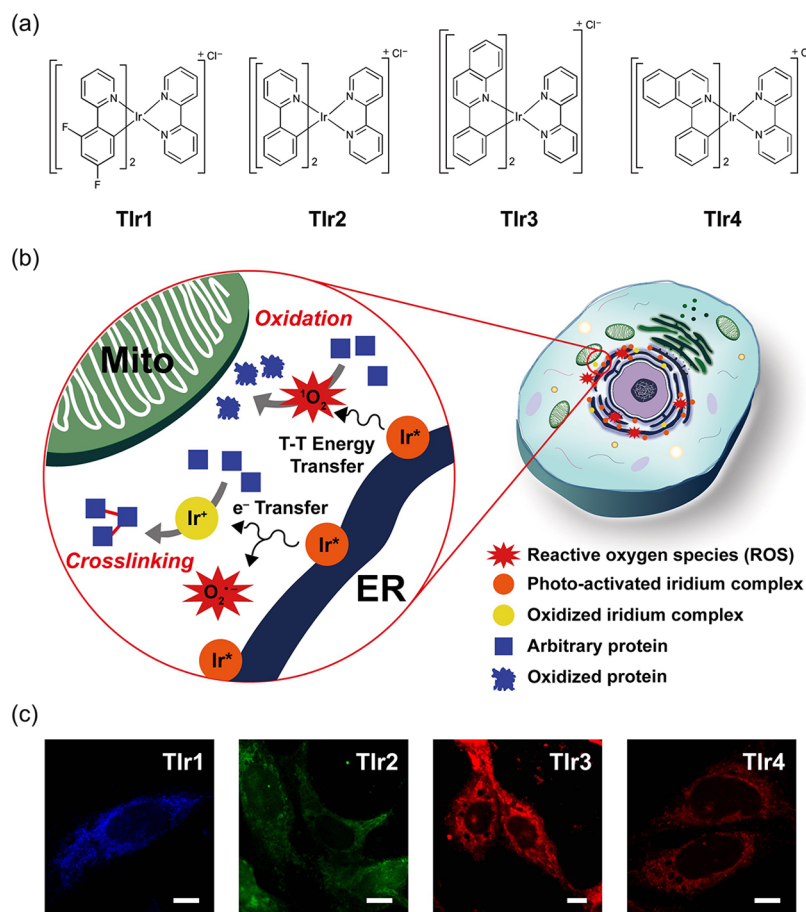


Figure 1. Protein modification pathways generated by Ir(III) complexes in cellular regions and optical imaging thereof. (a) Cyclometalated Ir(III) complexes, **Tlr1**, **Tlr2**, **Tlr3**, and **Tlr4**. (b) Schematic representation of protein modifications in the mitochondria (Mito) and endoplasmic reticulum (ER) by photoactivation of Ir(III) complexes. There are two expected pathways for protein modification, cross-linking and oxidation. (c) Two-photon optical imaging of **Tlr1**, **Tlr2**, **Tlr3**, and **Tlr4** (from left to right) using confocal laser scanning microscopy. Scale bar = 10 μm .

ideal conditions for an effective cancer therapy system because of the potential for deep-tissue imaging.¹³ Notably, these Ir(III) complexes were primarily localized in the endoplasmic reticulum (ER). Only **Tlr3** and **Tlr4** showed noticeable PDT activity for SK-OV-3 ovarian and MCF-7 breast cancer cells, likely because they efficiently produce ROS owing to their well-matched energy levels for $^1\text{O}_2$ generation and high Φ_p . Finally, we propose potential mechanisms clarifying prompt cell death via oxidation of essential proteins (e.g., TRAP1, PYCR1) in the ER and mitochondria and by arbitrary protein photo-cross-linking in the vicinity of the Ir(III) complexes without requiring toxic additives, leading to protein aggregation in living cells (Figure 1b).

RESULTS AND DISCUSSION

Ir(III) Complexes as Photodynamic Therapy (PDT) Agents. Developing effective PDT systems encompasses the following factors: light activation in the near-infrared (IR) region, high absorption coefficient, rapid and conspicuous imaging of cancer cells, and ROS generation capability. Considering these criteria, four cationic Ir(III) complexes (**Tlr1**–**4**; Figure 1a and Scheme S1) were designed and prepared. We expected that ROS generation would be dependent on the energy level of the photosensitizers because $^1\text{O}_2$ formation occurs by energy transfer. Thus, suitable energy overlaps between photosensitizers (energy donor) and O_2

(energy acceptor) in addition to high emission quantum yields would allow enhanced ROS production through controlling energy levels of the photosensitizers.¹⁴ Accordingly, four different ligands [difluorophenylpyridine (dfppy), 2-phenylpyridine (ppy), 2-phenylquinoline (2pq), and 1-phenylquinoline (1pq)] were incorporated into the Ir(III) center. Additionally, the bipyridine (bpy) ligand was employed as an ancillary ligand to afford overall cationic Ir(III) complexes that are soluble in aqueous systems while retaining their high emission quantum yields.¹⁵ To measure the energy bandgaps and extinction coefficients upon metal-to-ligand charge transfer (MLCT) of the Ir(III) complexes, the UV–visible (UV–vis) absorption spectra of **Tlr1**–**4** were measured (Figure 2a and Table 1), indicating MLCT at 350, 375, 448, and 450 nm, respectively, and the corresponding extinction coefficients (ϵ) (range 5587–6971 $\text{M}^{-1} \text{cm}^{-1}$) that are higher than that of HPD.⁵ The respective onset points of **Tlr1**–**4** on the UV–vis spectra corresponding to the energy bandgaps appear at 399, 428, 488, and 494 nm.

Cyclic voltammetry (CV) was conducted to measure the oxidation potentials (Figure 2b), corresponding to the highest occupied molecular orbital (HOMO) of the Ir(III) complexes. Based on the onset points of UV–vis and the oxidation potentials measured by CV, the singlet energy levels of the Ir(III) complexes were presented in Figure 2c, along with the corresponding energy bandgap order [**Tlr1** > **Tlr2** > **Tlr3** > **Tlr4**]. The maximum emission wavelengths (λ_{max}) correspond-

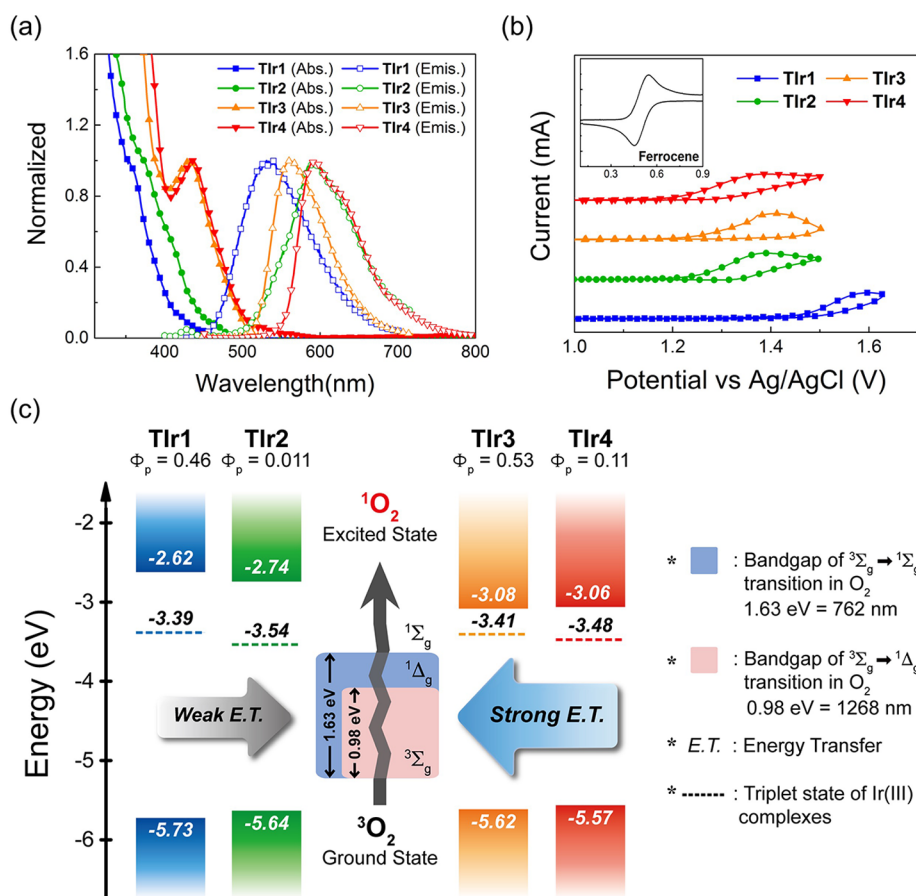


Figure 2. Optical and electrochemical properties of **Tlr1**, **Tlr2**, **Tlr3**, and **Tlr4** and correlation of their energy levels with the two singlet oxygen (1O_2) excitation state energies. (a) Normalized UV–visible (closed symbols) and photoluminescence (open symbols) spectra upon excitation in the MLCT region of **Tlr1**, **Tlr2**, **Tlr3**, and **Tlr4**. Condition: $[\text{Ir(III) complex}] = 20 \mu\text{M}$ concentration. (b) Cyclic voltammetry (CV) graph for each Ir(III) complex. Spectra were obtained with a 50 mV/s scan rate in tetrabutylammonium hexafluorophosphate (TBAPF_6^-) electrolyte dissolved in acetonitrile. (c) Energy level of each Ir(III) complex and ground state oxygen (1O_2) absorption. The HOMO was measured by the onset potential of the Ir(III) complex with a ferrocene reference (inset) using the following equation. $\text{HOMO} = -(E_{\text{onset-of-Ir(III)}} \text{ vs } E_{\text{onset-of-ferrocene}}) - 4.8 \text{ eV}$. The energy band gap was measured from the onset peak of the absorption spectrum and the LUMO was calculated as $\text{HOMO} + \text{energy band gap}$. Triplet energy levels corresponded with maximum emission peaks (dashed lines). Two excitation states of singlet oxygen ($^1\Sigma_g$ for 762 nm and $^1\Delta_g$ for 1268 nm) representing the absorption energy from ground state oxygen are presented.

Table 1. Photophysical and Electrochemical Properties for Each Complex

complex	λ_{abs}^a (nm)	λ_{emiss}^a (nm)	HOMO ^b (eV)	E_T (eV)	LUMO (eV)	Φ_p^c	Φ_s	lifetime ^d (ns)	k_r^e ($\times 10^5 \text{ s}^{-1}$)	k_{nr}^e ($\times 10^5 \text{ s}^{-1}$)
Tlr1	354	531	-5.73 (-5.81)	-3.39	-2.62	0.46 ± 0.02	0.32 ± 0.04	374	12.3	14.4
Tlr2	374	590	-5.64 (-5.56)	-3.54	-2.74	0.011 ± 0.001	0.37 ± 0.01	72	1.53	138
Tlr3	432	562	-5.62 (-5.61)	-3.41	-3.08	0.53 ± 0.05	0.95 ± 0.04	712	7.44	6.60
Tlr4	437	592	-5.57 (-5.60)	-3.48	-3.06	0.11 ± 0.01	0.78 ± 0.04	702	1.57	12.7
$[\text{Ru}(\text{bpy})_3]^{2+}$	453	611				0.063	0.18	398	1.58	23.5

^a λ_{abs} and λ_{emiss} were measured in aqueous media containing 1% DMSO (v/v). ^bHOMO energy levels were obtained by cyclic voltammetry under both organic (acetonitrile, MeCN) and aqueous (DI water containing 1% DMSO (v/v)) conditions. Tetrabutylammonium hexafluorophosphate (TBAPF_6^-) and potassium chloride (KCl) were utilized as supporting electrolytes for organic and aqueous conditions, respectively. The HOMO values in parentheses indicate HOMO energy levels in aqueous solution. ^cQuantum yields were measured in aqueous media containing 1% DMSO (v/v) with the reference of Flrpic for **Tlr1**, $(\text{ppy})_2\text{Irpic}$ for **Tlr2**, and $(2\text{pq})_2\text{Ir}(\text{ppy})^+\text{PF}_6^-$ for both **Tlr3** and **Tlr4**. Standard deviation was obtained from three measurements. Quantum yield of $[\text{Ru}(\text{bpy})_3]^{2+}$ is taken from the ref 41. ^dTime-correlated single photon counting (TCSPC) measurement confirmed excited state lifetime of **Tlr1**, **Tlr2**, **Tlr3**, **Tlr4**, and $[\text{Ru}(\text{bpy})_3]^{2+}$. ^eRadiative decay constant (k_r) and nonradiative decay constant (k_{nr}) were calculated with previously reported equations.⁴²

ing to the triplet energy levels of Ir(III) complexes were measured by photoluminescence spectroscopy and, when excitation was performed at the MLCT, they are indicated to be at 531, 590, 562, and 592 nm for **Tlr1**–**4**, respectively (Figure 2a). The triplet emission from **Tlr2** was highly dependent on the solvent polarity; therefore, a large Stokes

shift appears in water compared with that in organic solvents (data not shown). Furthermore, Φ_p of the Ir(III) complexes was observed to be highly dependent on their ligands [**Tlr3** (0.53 ± 0.05) > **Tlr1** (0.46 ± 0.02) > **Tlr4** (0.11 ± 0.01) > **Tlr2** (0.011 ± 0.001)]. Additionally, all Ir(III) complexes present two-photon absorption properties. The two-photon

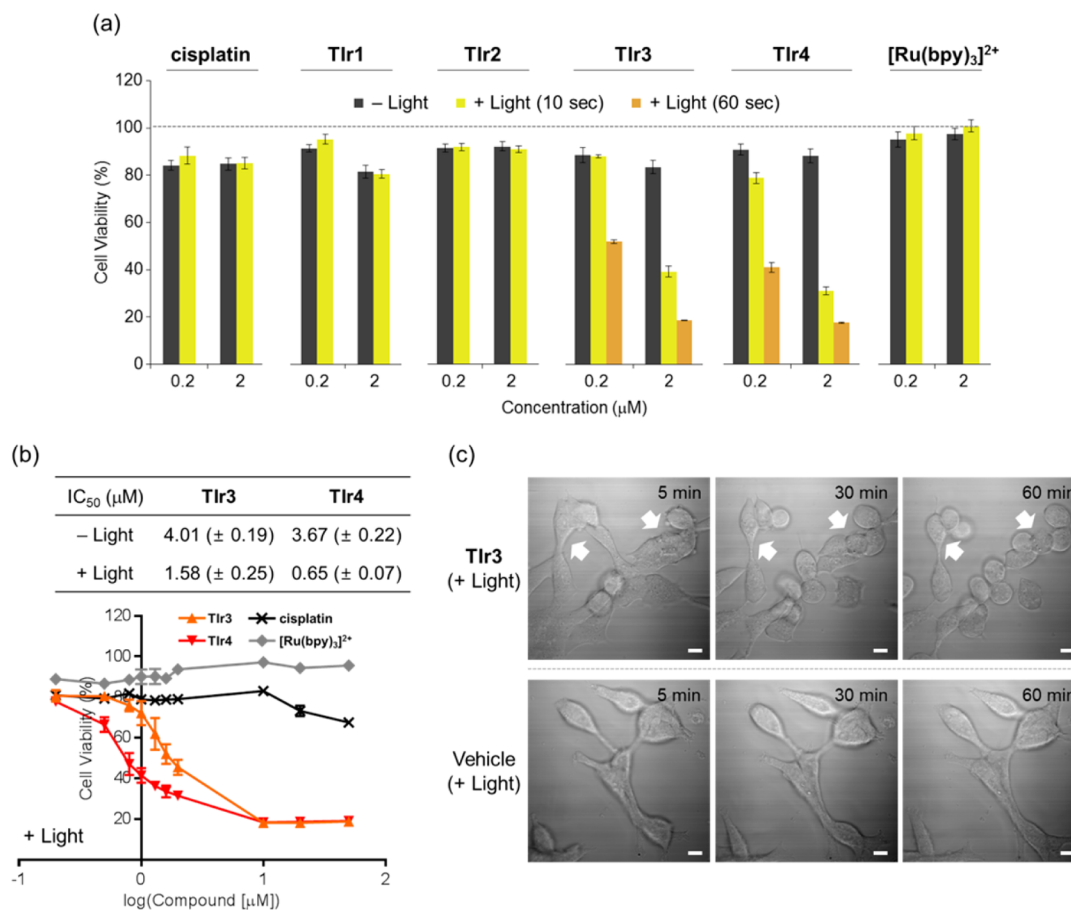


Figure 3. Cell death triggered by Ir(III) complexes and real time tracking of cell morphological alteration. (a) Viability of human ovarian cancer SK-OV-3 cells upon treatment with Ir(III) complexes, cisplatin, and $[\text{Ru}(\text{bpy})_3]^{2+}$ [IC_{50} values of **Tlr3** and **Tlr4** in the absence and presence of 1 sun light (100 mW cm^{-2}) for 10 s (b, top)]. Plots of cell viability as a function of $\log(\text{concentration of complexes})$ upon light treatment [$1 \text{ sun light } (100 \text{ mW cm}^{-2})$ for 10 s] (b, bottom). Cytotoxicity was measured by the MTT assay after 24 h incubation of SK-OV-3 cells with and without light exposure. The cell viability (%) was calculated compared with cells treated with equivalent amounts of dimethyl sulfoxide (DMSO) or dimethylformamide (DMF) only (1%, v/v). Values represent the mean of three independent experiments. (c) Change of cell morphologies upon treatment with **Tlr3** with two-photon activation. Morphological changes of **Tlr3**-added (top, [**Tlr3**] = $20 \mu\text{M}$) and vehicle-treated (bottom) SK-OV-3 cells after two-photon photoirradiation ($\lambda = 860 \text{ nm}$ for 30 s). Scale bar = $10 \mu\text{m}$.

excitation spectra, similar to the UV-vis absorption spectra, range from 670 to 950 nm, which is an appropriate near-IR range wherein living cells would not be damaged by high-energy excitation light. The emission spectra and nonlinear properties for two-photon absorption are depicted in [Supporting Information Figures S1 and S2](#).

Images of the HeLa cells upon incubation with each Ir(III) complex were further obtained by two-photon laser scanning microscopy. All Ir(III) complexes emit noticeable phosphorescence even at a relatively low concentration ($10 \mu\text{M}$) upon incubation for 30 min ([Figure 1c](#)). Our imaging investigations clearly demonstrate the cell-membrane permeability of each Ir(III) complex and the accompanying critical localization to the ER vicinity. Furthermore, fluorescence lifetime imaging microscopy (FLIM) analysis confirmed the extended **Tlr3** phosphorescence (ca. 500 ns) in the vicinity of ER compared with the short lifetime (ca. 5 ns) of a nuclear-localized fluorescent protein (H2B-mCherry) ([Supporting Information Figure S3](#)). This long lifetime could result from the relatively strong spin-orbit coupling by iridium,¹⁶ which can boost the possibility of electron or energy transfer from Ir(III) complexes to O_2 , resulting in more efficient ROS generation.

Cytotoxicity Evaluation of Light-Activated Ir(III) Complexes. The PDT potency for **Tlr1–4** was monitored in SK-OV-3 ovarian and MCF-7 breast cancer cells via the 3-(4,5-dimethylthiazol-2-yl)-2,5-diphenyl tetrazolium bromide (MTT) assay and compared with that of a well-known anticancer drug, cisplatin,¹⁷ and a reported photoactivatable reagent, $[\text{Ru}(\text{bpy})_3]^{2+}$ ([Figure 3a](#) and [Supporting Information Figure S4](#)).¹⁸ Cell viability upon treatment with a relatively low concentration of **Tlr3** (i.e., $2 \mu\text{M}$) where it could be still photoactivated was markedly reduced to 40% and 19%, respectively, with 10 and 60 s irradiation ([Figure 3a](#)); **Tlr4** displayed similar effect on cell viability to **Tlr3** (31% and 18% cell viability for the samples treated 10 and 60 s irradiation, respectively). Without light, cell death was not significantly triggered by **Tlr3** (89% and 84% cell viability for 0.2 and $2 \mu\text{M}$, respectively) or **Tlr4** (91% and 89% cell viability for 0.2 and $2 \mu\text{M}$, respectively). Furthermore, a submicromolar complex concentration (i.e., $0.2 \mu\text{M}$) diminished the survival of SK-OV-3 cells to 52% and 41% for **Tlr3** and **Tlr4**, respectively, after 60 s of light exposure ([Figure 3a](#)). These influential PDT effects were observed in MCF-7 cells as well ([Supporting Information Figure S4a](#)). In addition, IC_{50} values of **Tlr3** and **Tlr4** were summarized in [Figure 3b](#) (SK-OV-3 cells) and [Supporting](#)

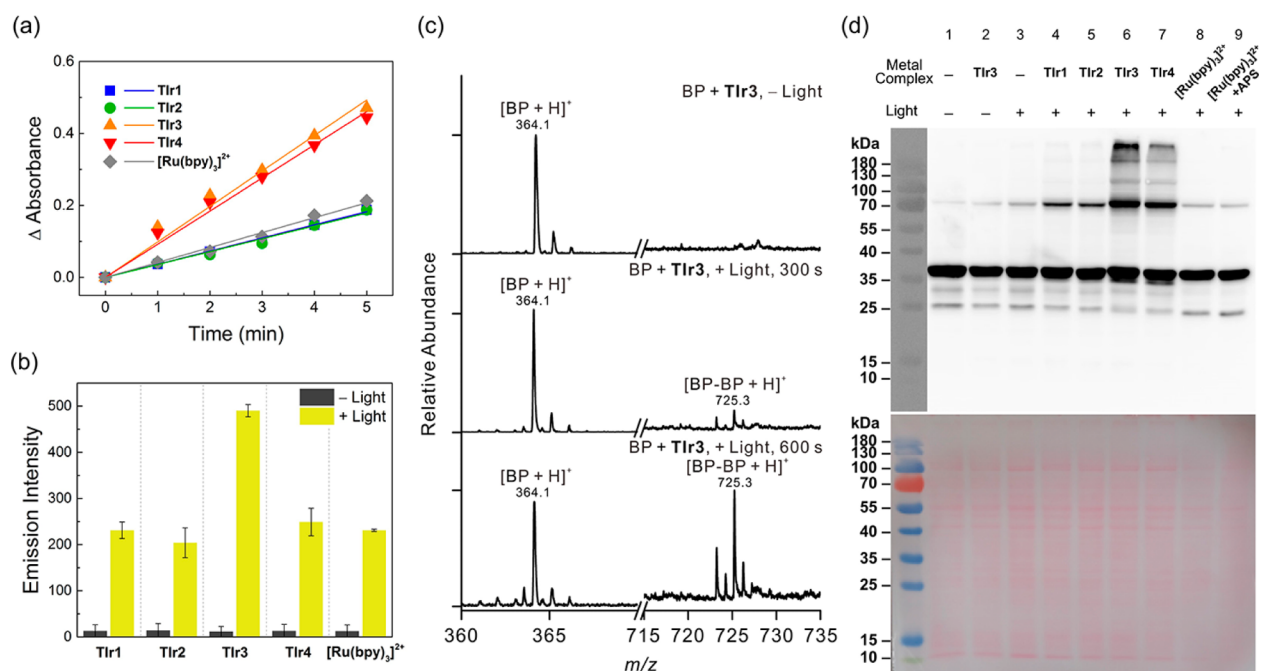


Figure 4. Two different ROS assays and photo-cross-linking analysis *in vitro* (biotin phenol (BP)) and in HEK293T cell culture. (a) Singlet oxygen ($^1\text{O}_2$) assay using the absorbance attenuation ($\Delta A = A_s - A_t$) of 9,10-anthracenediyl-bis(methylene)dimalonic acid (ABDA) under light exposure. The slope corresponds to the absolute amount of $^1\text{O}_2$. (b) Superoxide anion radical ($\text{O}_2^{\bullet-}$) assay indicating the enhancement in fluorescence by conversion of dihydrorhodamine 123 to rhodamine 123. (c) Dimerization of biotin-phenol by **T1r3**, as monitored by MALDI-MS. Conditions: $[\text{BP}] = 500 \mu\text{M}$; $[\text{T1r3}] = 1 \text{ mM}$; 100 mW cm^{-2} light; irradiation time = 0, 300, and 600 s. (d) Analysis of photo-cross-linking in living cells by metal complexes (top) and Ponceau S staining for identifying protein loading quantities (bottom). Conditions: $[\text{metal complex}] = 2 \mu\text{M}$; $[\text{APS}] = 50 \mu\text{M}$; 100 mW cm^{-2} light; irradiation time = 60 s.

Information Figure S4b (MCF-7 cells). **T1r3** and **T1r4** showed 4.01/1.58 and 3.67/0.65 μM IC_{50} values without and with light, respectively, in SK-OV-3 cells (Figure 3b); similarly, in MCF7 cells, 4.89/0.83 and 3.61/0.63 μM IC_{50} values were presented for **T1r3** and **T1r4** in the absence or presence of light, respectively (Supporting Information Figure S4b). For cisplatin and $[\text{Ru}(\text{bpy})_3]^{2+}$, IC_{50} values were not indicated up to 50 μM of each complex in both cell lines. In contrast to **T1r3** and **T1r4**, the PDT activity for **T1r1**, **T1r2**, $[\text{Ru}(\text{bpy})_3]^{2+}$, and cisplatin was not noticeable regardless of light control under our experimental conditions (Figure 3a and Supporting Information Figure S4). Overall, our studies indicate the potential of **T1r3** and **T1r4** to serve as PDT agents simply using 1 sun light (100 mW cm^{-2} light; 1 J cm^{-2}) just for 10 s, thus requiring much lower energy than previously reported Ir(III) complexes ($12\text{--}36 \text{ J cm}^{-2}$).¹⁹

The potential use of **T1r3** as a two-photon-based PDT agent was further investigated by visualizing the morphological changes of SK-OV-3 cells upon co-incubation. Cell shrinkage was clearly indicated by **T1r3** treatment as a function of time (5, 30, and 60 min) upon irradiation at 860 nm (Figure 3b). In contrast, no morphological alteration occurred in the absence of **T1r3** even with irradiation. Thus, our Ir(III) complexes (particularly **T1r3**) demonstrate the potential as PDT agents employing either one- or two-photon irradiation.

Characterization of ROS Generation by Ir(III) Complexes. The ROS generation ability of Ir(III) complexes according to their energy levels was identified by three different analyses: triplet state quenching by O_2 , 9,10-anthracenediyl-bis(methylene) malonic acid (ABDA) assay for $^1\text{O}_2$ generation,²⁰ and dihydrorhodamine (DHR) 123 assay for superoxide radical ($\text{O}_2^{\bullet-}$) generation.²¹ Triplet state quenching of

Ir(III) complexes by O_2 bubbling relates to the amount of formed ROS, because it strongly depends on $^1\text{O}_2$ generation and charge transfer interactions from Ir(III) complexes to O_2 , resulting in oxygen radical formation.²² The quenching rate order is **T1r3** > **T1r4** > **T1r1** > $[\text{Ru}(\text{bpy})_3]^{2+}$ > **T1r2** (Supporting Information Figure S5), suggesting that **T1r3** is the best photoactivatable ROS generator for PDT in our system.

Next, the Φ_s of Ir(III) complexes was obtained using the absorbance change (ΔA) of ABDA according to the irradiation time from 0 to 5 min with $[\text{Ru}(\text{bpy})_3]^{2+}$ ($\Phi_s = 0.18$ in H_2O) as a reference (Figure 4a and Supporting Information Figure S6).²³ **T1r3** showed the highest Φ_s (0.95 ± 0.04) followed by **T1r4** (0.78 ± 0.04), **T1r2** (0.37 ± 0.01), and **T1r1** (0.29 ± 0.04) (Table 1). $^1\text{O}_2$ generation relies upon energy transfer; thus, it is closely related to the difference in the energy level between the energy donor and acceptor, as well as to the emission quantum yield of the energy donor. Previously, it is reported that one guideline of the oxidation potential of sensitizer for efficient PDT properties is 1.10 V vs SCE (= 1.34 V vs NHE), which corresponds to -5.51 eV of HOMO,²⁴ and deeper HOMO is preferable.²⁵ To enhance the energy transfer, the HOMO of the energy donor has a lower (down shift) energy than that of energy acceptor, and all of our Ir(III) complexes satisfied this condition under both organic and aqueous media (Table 1). Additionally, O_2 as an energy acceptor has two singlet excited states with corresponding absorption energies of 762 and 1268 nm.^{18,24} Matching of these energy levels is critical for efficient energy transfer; therefore, the minimum triplet energy of Ir(III) complexes should be higher than 762 nm (i.e., 1.63 eV). Conversely, excessively high triplet energy [e.g., **T1r1**; 531 nm (i.e., 2.34 eV)] leads to

inefficient energy transfer because of mismatch with the energy level of O_2 .²⁴

If the energy level is well-matched, the emission quantum yield should also be considered.¹⁴ For example, both **TIr3** (562 nm, 2.21 eV) and **TIr4** (592 nm, 2.09 eV) had appropriate energy levels for efficient energy transfer toward ground-state O_2 . **TIr3** exhibits the highest Φ_s (0.95), followed by **TIr4** ($\Phi_s = 0.78$), because of its higher Φ_p (0.53 vs 0.11). Although Φ_p of **TIr1** is high (0.46), its Φ_s is the lowest (0.29) because of mismatched energy levels. **TIr2** has a reasonable triplet energy (590 nm, 2.10 eV); however, it has a lower Φ_s (0.37) because of its minimal Φ_p (0.01). To confirm these calculated predictions, we prepared four neutral (**Neutral-1–4**) and three anionic (**Anionic-1–3**) Ir(III) complexes by substituting the ancillary ligand while retaining the main ligand. These complexes exhibited the same results as the cationic species (from **TIr1** to **TIr4**). The highest Φ_p and appropriate energy level (> 1.63 eV) of the Ir(III) complexes generated 1O_2 efficiently (Supporting Information Figure S7).

Based on these findings, we propose that for efficient generation of 1O_2 , Ir(III) sensitizers should have an energy band gap between 1.63 and 2.21 eV as a major factor, a high emission quantum yield, and a reasonable HOMO energy (lower position than -5.51 eV). In the DHR 123 assay, the relative rates for $O_2^{\bullet-}$ production are in order of **TIr3** \gg **TIr4** $>$ **TIr1** = $[Ru(bpy)_3]^{2+}$ $>$ **TIr2** (Figure 4b), corresponding to 1O_2 generation. Taken together, our studies of ROS generated by Ir(III) complexes indicate that **TIr3** exhibits relatively high oxygen sensitivity, resulting in its relatively high Φ_s and generation of $O_2^{\bullet-}$, with subsequent photocontrolled cytotoxicity.

Characterization of Protein Cross-Linking by Ir(III) Complexes. Following these ROS generation analyses, we evaluated the efficiency of the Ir(III) complex for photoinduced protein cross-linking, which could inactivate protein physiological functions by aggregation, potentially generating additional cytotoxicity.²⁶ $[Ru(bpy)_3]^{2+}$ systems require an exogenous additive such as ammonium persulfate (APS) as an electron acceptor for initiating cross-linking pathways²⁷ and might have not been applied in PDT because of the toxicity of APS. Thus, fast and efficient additive-free protein cross-linking reagents would be valuable for PDT development.

Generally, photoactivated protein cross-linking by metal complexes occurs through coupling reactions with tyrosyl radicals exposed on the protein surfaces.²⁷ We utilized biotin-phenol (BP), which has a tyrosine residue, to confirm covalent dimerization by *in vitro* cross-linking with photoactivation of metal complex. BP cross-linking induced by metal complexes was confirmed by matrix-assisted laser desorption ionization mass spectrometry (MALDI-MS). For **TIr3**, the cross-linked BP (BP–BP + H^+ , m/z 725.3) was clearly observed in the presence of O_2 with light exposure (Figure 4c), whereas it was not generated without either O_2 or light (Figure 4c and Supporting Information Figure S8). BP cross-linking using $[Ru(bpy)_3]^{2+}$ also occurred only in the presence of APS with O_2 and light (Supporting Information Figure S9). These results suggest that **TIr3**, in contrast to $[Ru(bpy)_3]^{2+}$, is able to achieve cross-linking in the presence of O_2 and light without requirement of an exogenous additive.

We also investigated whether our Ir(III) complexes could induce protein–protein cross-linking in living cells. We transiently expressed the GFP-Sec61B protein, which localizes at the ER cytosolic membrane, and conducted photo-cross-

linking experiments with **TIr1–4** and $[Ru(bpy)_3]^{2+}$. Western blot results with an anti-GFP demonstrated substantial protein–protein cross-linking (over 180 kDa) by **TIr3** and **TIr4**, which were more effective upon light activation (Figure 4d, lanes 6 and 7). For **TIr1** (lane 4) and **TIr2** (lane 5), only mild cross-linking was observed. Cross-linking by the Ir(III) complexes occurred only with light illumination. Note that **Neutral-3** and **Anionic-3** as a representative of neutral and anionic Ir(III) complexes (Supporting Information Figure S7) did not generate photo-cross-linked product efficiently, compared with **TIr1** and **TIr3** (Supporting Information Figure S10). Notably, no efficient protein cross-linking was indicated with $[Ru(bpy)_3]^{2+}$, even with APS treatment (Figure 4d, lanes 8 and 9), suggesting limited applications in living cells. Overall, our Ir(III) complexes are demonstrated to be better protein photo-cross-linking reagents than $[Ru(bpy)_3]^{2+}$ both *in vitro* and in living cells, and they do not include toxic additives, implying suitability for use in the cellular environment. We postulate that the higher performance of Ir(III) complexes might be derived from their oxygen sensitivity and extended excitation lifetime (Table 1), implying efficient charge transfer and energy transfer because of minimized nonradiative decay.

Identification of Oxidative Modifications of Endogenous Proteins by TIr3. In addition to protein–protein cross-linking, we attempted to identify whether protein oxidation could be achieved by **TIr3**. In our analysis of protein oxidation, we focused on modified proteins that contain oxidized methionine residues, since mono-oxidized methionine (O-Met, Met +16 Da) has been characterized as the major oxidative product by ROS and recent proteomic profiling studies have shown that over 2000 oxidized methionine sites are globally generated when cells are exposed to hydrogen peroxide (H_2O_2).²⁸ By using **TIr3**, we expected to observe focused O-Met sites in proteins proximal to subcellularly localized **TIr3** that could be directly affected by **TIr3**-generated 1O_2 *in situ*, which has a lifetime of less than 1 ms.²⁹ This mapping would enable the detection of specific proteins oxidatively damaged by our PDT agents, potentially leading to improved understanding of the underlying biological events.

To identify the additional oxidation by the **TIr3**, we used methionine sulfoxide antibody, and it showed that **TIr3** and **TIr4** generated more oxidized proteins than negative controls (Supporting Information Figure S11). Surprisingly, Western blot pattern of methionine-oxidized proteins resembled that of photo-cross-linked products. This result implies that photo-oxidation and photo-cross-linking reactions by **TIr3** and **TIr4** might simultaneously occur on the same substrate proteins. Other Ir(III) complexes showed similar level of oxidized proteins relative to basal level of the negative controls (Supporting Information Figure S11). This result indicates that other iridium complexes performed negligible photo-oxidation on the endogenous proteins in a living cell. From this result, we selected **TIr3** sample for profiling of photo-oxidized proteins by mass spectrometry analysis.

Three samples containing **TIr3** with light illumination, as well as the three other samples as negative controls (control sample; #1, without light; #2, without **TIr3**; #3, without both light and **TIr3**), were prepared. The cells were lysed in RIPA buffer and digested with trypsin after loading in SDS-PAGE gel. The peptides were desalted and analyzed using LTQ-Orbitrap mass spectrometry. The analyzed peptides were first filtered by O-Met (Met +16 Da) modification, and the modified peptides were second filtered by reproducible observation of the same

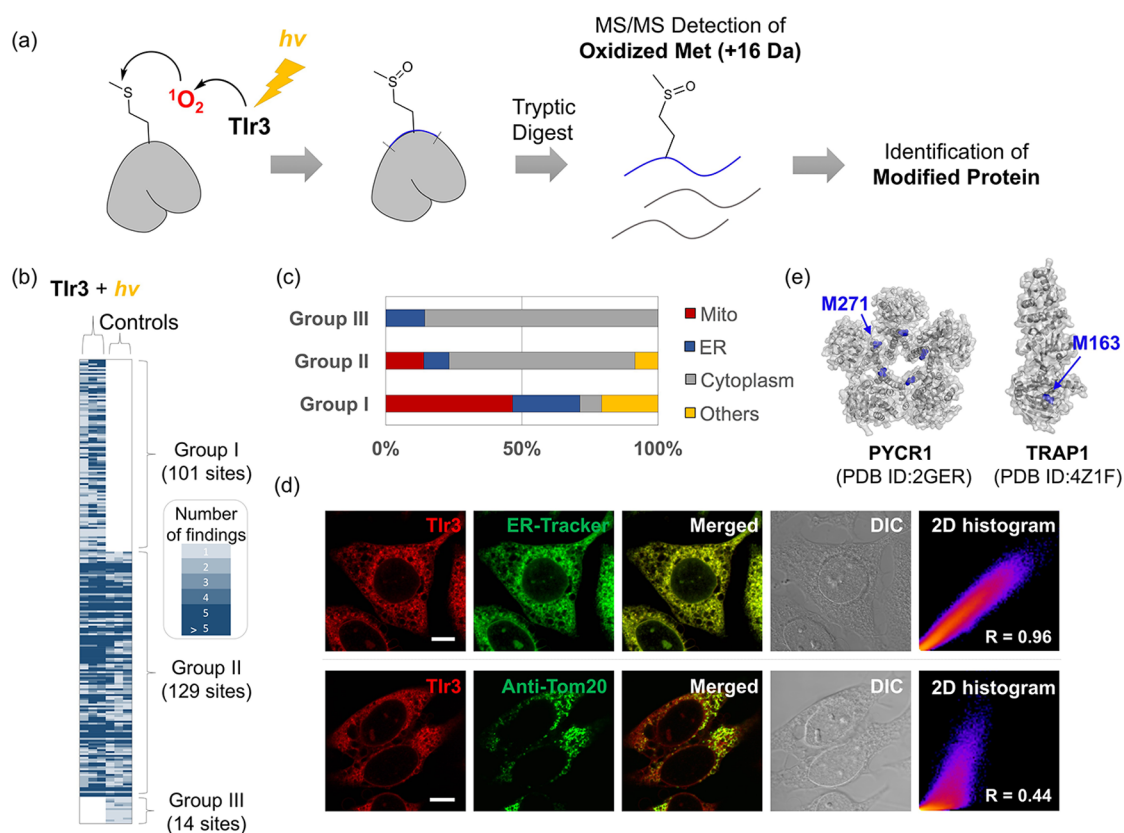


Figure 5. Identification of the oxidative damage to the proteome induced by **Tlr3** upon photoactivation through MS/MS detection of methionine oxidation (+ 16 Da) and primary localization of **Tlr3** cell organelle labeling. (a) Schematic representation of the experimental process for identification of oxidized proteins by MS. (b) Proteomic profiling of proteins oxidized on methionine residues (group I, additionally oxidized species by **Tlr3**; groups II and III, oxidized species by endogenously generated ROS). (c) Distribution ratio of oxidized proteins for each group. **Tlr3** accelerates the oxidation of proteins localized in the mitochondria and ER. (d) Confocal microscopy imaging ($\lambda_{em} = 560$ nm) of HeLa cells labeled with **Tlr3** (10 μ M, 0.5 h) and its colocalization with ER-Tracker or Anti-Tom20; 2D histogram graph indicates degree of colocalization, implying Pearson's coefficient (R). Note that Anti-Tom20 was obtained in AF647 window; thereby green is false color. Scale bar = 10 μ m. (e) Crystal structure of representative oxidized proteins. Both proteins play a role in mitochondrial function.

O-Met sites three times, either in PDT-treated triplicates or in the three negative control samples. Finally, a total of 244 O-Met sites were identified in our study; 101 O-Met sites were exclusively observed in PDT-treated triplicates (group I) and 129 O-Met sites were consistently observed both in PDT-treated sample and negative samples (group II) (Figure 5b). Thus, group II sites can be regarded as endogenous oxidized methionine residues regardless of photo-oxidation, and group I sites can be considered to be additionally generated O-Met from the photodynamic reaction by **Tlr3**. We also noted 14 O-Met sites that were exclusively observed in the control samples (group III).

When these O-Met sites were mapped onto the subcellular compartments, such as mitochondria, ER, and cytoplasm (Figure 5c), significant numbers of group I sites were mapped onto mitochondrial proteins (47 out of 101 sites) and a considerable number were mapped onto ER proteins (25 out of 101 sites). This is a rather surprising result compared with the subcellular population of group II sites, in which the majority of modified sites were mapped onto cytoplasmic proteins (88 out of 129 sites) composed of cytoskeleton proteins such as actin (e.g., ACTB, ACTC1), tubulin (e.g., TUBA1C, TUBB2B, TUBB4B), and heat-shock proteins (e.g., HSP90AA1, HSP90AB1, HSP90B1, HSPA1A, HSPA4, HSPA5, HSPA8, HSPA9) that are known to readily modify O-Met by the endogenously generated ROS.³⁰ In contrast, a small number of

modified sites were mapped onto mitochondrial proteins (18 out of 129 sites) and ER proteins (12 of 129 sites). Similarly, the majority of group III (12 out of 14) were mapped onto cytoplasmic proteins, especially actin proteins (e.g., ACTB, ACTC1, ACTG1), which are known to be readily oxidized by endogenous ROS.³⁰ Groups II and III showed similar subcellular localized population, and the total spectral count of group III sites was significantly lower than that of group I or II. Thus, we postulated that group III sites should be endogenously oxidized Met residues and that they might be excluded during the mass analysis of other abundant O-Met-modified peptides in PDT-treated samples. Overall, the spatially resolved protein oxidation by **Tlr3** with photoactivation clearly occurred at the mitochondria and ER, indicating **Tlr3** should be localized at these subcellular compartments.

Primary Subcellular Localization of Tlr3 in Living Cells. To determine the subcellular localization of **Tlr3**, we imaged **Tlr3** localized region in HeLa cell and HEK293T cell line, respectively. ER tracker dyes for ER staining³¹ and immunofluorescence of anti-Tom20, which shows mitochondrial pattern, were employed to confirm the subcellular localization pattern of **Tlr3**.³² Noticeably, the resultant images clearly indicated that the **Tlr3** staining region substantially overlapped with ER-Tracker (Pearson correlation value = 0.96, Figure 5d) while it partially overlapped with immunofluor-

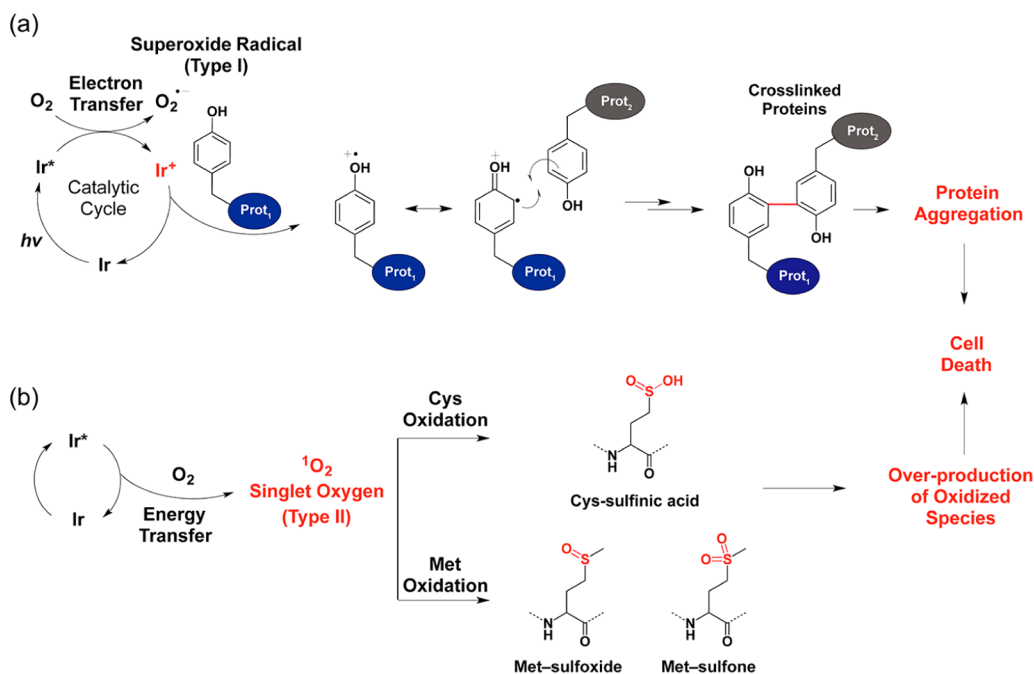


Figure 6. Proposed modes of action of Ir(III) complexes for photodynamic therapy (PDT). (a) Photo-cross-linking pathway through a catalytic cycle initiated by a one-electron process from the Ir(III) complex to O₂, which can result in cell death via protein aggregation. (b) Protein oxidation pathway from ¹O₂ by triplet-triplet energy transfer of the excited state of the Ir(III) complex. Overexpression of oxidized proteins also induces cell death.

escence of anti-Tom20 (Pearson correlation value = 0.44, Figure 5d). Additionally, we confirmed that TIr3 was mainly localized at the ER and partially overlapped with mitochondria in HEK293T cell line (Supporting Information Figure S13). TIr1, TIr2, and TIr4 also showed well overlapped localized pattern with ER-Tracker in both HeLa and HEK293T cell lines (Supporting Information Figures S12 and S13).

These observations might be explained by our results that the major population of oxidized proteins by TIr3 was found in mitochondrial proteins (Figure 5c). The ER and mitochondria are interconnected within a few nanometers at the ER-mitochondria-tethered junction.³³ A fraction of ¹O₂ also reaches the mitochondrial space through the outer mitochondrial membrane, which allows passage of small molecules of less than 5 kDa.³⁴ Thus, we postulated that *in situ* generated ¹O₂ by TIr3 at the ER membrane might be diffused into the mitochondrial membrane and oxidized both proximal ER and mitochondrial proteins. We also observed that photo-oxidation reaction by TIr3 initiated mitochondrial aggregation, which is associated with the mitochondrial pathway of apoptosis (Supporting Information Figure S14).³⁵ Consequently, our imaging studies imply that our Ir(III) complexes, representing predominantly ER-localized PDT agents, could induce protein modifications (i.e., protein-protein cross-linking and protein oxidation) at both the ER and mitochondria upon light activation.

Oxidation of Mitochondrial Proteins Related to Mitochondrial Physiology by TIr3. Oxidized methionine is known to be more hydrophilic than methionine, and O-Met could form hydrogen bonds with other amino acid residues.³⁶ Thus, a significant conformation change could be triggered, affecting endogenous protein function and interactions with their partners.³⁷ Among 41 oxidized mitochondrial proteins in group I, TRAP1 was found to be oxidized by TIr3. TRAP1 is a mitochondrial matrix localized molecular chaperone protein³⁸ and serves as an oxidative sensor inducing apoptosis when it is

oxidized under oxidative stress.³⁹ Moreover, we also observed that PYCR1 involved in proline metabolism was oxidized by TIr3. Mutation of PYCR1 significantly affects mitochondrial morphology and membrane potential and increases apoptosis rate.⁴⁰ Thus, we postulate that O-Met modification of PYCR1 might cause a similar effect on the mitochondrial physiology (Figure 5e). Similarly, in group I, we found 15 other mitochondrial metabolic proteins that were related to human disease (e.g., HIBCH, TUFM, ACAT1, AK2, ADH7A1, CYCS, HADH, HADHA, HSD17B10, LRPPRC, OAT, PDHA1, SLC25A3) and were severely oxidized by TIr3, which might have altered their structures and affected mitochondrial function. Taken together, the photo-oxidation of proteins near the mitochondrial space by TIr3 can be utilized to effectively prompt cell death, demonstrating the Ir(III) complex as a promising PDT agent.

Proposed Mode of Action of Ir(III) Complexes as PDT Agents. Higher-ordered protein-protein cross-linking as triggered by our Ir(III) complexes can further induce protein aggregation. Additionally, excessive oxidation occurs on amino acid residues such as cysteine and methionine consequent to noticeable ROS generation, inducing protein dysfunction by structural change. As depicted in Figure 6, the induction of these two pathways by our Ir(III) complexes can accelerate cell death through a synergetic effect, suggesting their high potential to be utilized for PDT.

CONCLUSIONS

We developed PDT agents composed of Ir(III) complexes for cancer cells via a molecular design strategy for efficient ROS generation that accounted for appropriate energy levels and high emission quantum yields. TIr3 and TIr4 effectively triggered the death of cancer cells through spatiotemporal cytotoxic activity via their ROS generation ability ($\Phi_s = 0.95$ and 0.78, respectively) localized at the ER, even under low

concentration ($\leq 2 \mu\text{M}$) and weak light energy ($\leq 1 \text{ J cm}^{-2}$). Additionally, Tlr3 efficiently induced cancer cell death by two-photon irradiation. Using MS, we characterized the modes of action for Ir(III) complexes for both protein cross-linking and protein oxidation. In living cells, the damage was predominantly found in proteins near the ER and mitochondria with significant association to cell death pathways. Therefore, these Ir(III) complexes efficiently functioned as PDT agents in cancer cells. Further optimization of these Ir(III) photosensitizers could lead to rapid cell death following effective protein disablement. Additionally, our Ir(III) complexes could be used for additive-free photo-cross-linking in other fields beyond PDT.

■ ASSOCIATED CONTENT

Supporting Information

The Supporting Information is available free of charge via the Internet at The Supporting Information is available free of charge on the ACS Publications website at DOI: 10.1021/jacs.6b05302.

Raw data for identification of proteins altered by the Ir(III) complexes (XLSX)

Detailed procedures for the synthesis of the four Ir(III) complexes, photochemical studies, cell culturing and transfection, cell imaging for both one-/two-photon and FLIM, MALDI-TOF-MS analysis of *in vitro* BP photo-cross-linking, Western blotting for photo-cross-linking in living cells and oxidation analysis by LTQ-Orbitrap MS (PDF)

■ AUTHOR INFORMATION

Corresponding Authors

*mhl@unist.ac.kr

*rhee@unist.ac.kr

*kwon90@unist.ac.kr

Author Contributions

J.S.N., M.-G.K., J.K., and S.-Y.P. contributed equally to this work.

Notes

The authors declare no competing financial interest.

■ ACKNOWLEDGMENTS

This research was supported by the Ulsan National Institute of Science and Technology research fund (Grant 1.150117.01 to T.-H.K. and H.-W.R. and Grants 1.140101.01 and 1.160001.01 to T.-H.K., H.-W.R., and M.H.L.). J.K. acknowledges the support from the Global Ph.D. fellowship program through the National Research Foundation of Korea (NRF) funded by the Ministry of Education (Grant NRF-2015H1A2A1030823). S.-Y.P. and O.H.K. acknowledge the Institute for Basic Science (Grant IBS-R020-D1), Korea.

■ REFERENCES

- (1) Moan, J.; Peng, Q. *Anticancer Res.* **2003**, *23*, 3591.
- (2) Dolmans, D.; Fukumura, D.; Jain, R. K. *Nat. Rev. Cancer* **2003**, *3*, 380.
- (3) Kelly, J.; Snell, M. J. *Urol.* **1976**, *115*, 150.
- (4) Gomer, C. J.; Razum, N. J. *Photochem. Photobiol.* **1984**, *40*, 435.
- (5) Triesscheijn, M.; Baas, P.; Schellens, J. H. M.; Stewart, F. A. *Oncologist* **2006**, *11*, 1034.
- (6) (a) Gollnick, S. O.; Liu, X. N.; Owczarczak, B.; Musser, D. A.; Henderson, B. W. *Cancer Res.* **1997**, *57*, 3904. (b) deVree, W. J. A.;

Essers, M. C.; deBruijn, H. S.; Star, W. M.; Koster, J. F.; Sluiter, W. *Cancer Res.* **1996**, *56*, 2908.

- (7) Kelland, L. *Nat. Rev. Cancer* **2007**, *7*, 573.
- (8) Frei, A.; Rubbiani, R.; Tubafard, S.; Blacque, O.; Anstaett, P.; Felgentrager, A.; Maisch, T.; Spiccia, L.; Gasser, G. *J. Med. Chem.* **2014**, *57*, 7280.
- (9) Hergueta-Bravo, A.; Jimenez-Hernandez, M. E.; Montero, F.; Oliveros, E.; Orellana, G. *J. Phys. Chem. B* **2002**, *106*, 4010.
- (10) Li, S. P. Y.; Lau, C. T. S.; Louie, M. W.; Lam, Y. W.; Cheng, S. H.; Lo, K. K. W. *Biomaterials* **2013**, *34*, 7519.
- (11) (a) You, Y. *Curr. Opin. Chem. Biol.* **2013**, *17*, 699. (b) Gao, R.; Ho, D. G.; Hernandez, B.; Selke, M.; Murphy, D.; Djurovich, P. I.; Thompson, M. E. *J. Am. Chem. Soc.* **2002**, *124*, 14828.
- (12) Liu, Z.; Sadler, P. J. *Acc. Chem. Res.* **2014**, *47*, 1174.
- (13) (a) Cho, S.; You, Y.; Nam, W. *RSC Adv.* **2014**, *4*, 16913. (b) Zheng, X. C.; Tang, H.; Xie, C.; Zhang, J. L.; Wu, W.; Jiang, X. Q. *Angew. Chem., Int. Ed.* **2015**, *54*, 8094.
- (14) (a) Hardin, B. E.; Hoke, E. T.; Armstrong, P. B.; Yum, J. H.; Comte, P.; Torres, T.; Frechet, J. M. J.; Nazeeruddin, M. K.; Gratzel, M.; McGehee, M. D. *Nat. Photonics* **2009**, *3*, 406. (b) Yun, M. H.; Lee, E.; Lee, W.; Choi, H.; Lee, B. R.; Song, M. H.; Hong, J. I.; Kwon, T. H.; Kim, J. Y. *J. Mater. Chem. C* **2014**, *2*, 10195.
- (15) Zhao, Q.; Yu, M.; Shi, L.; Liu, S.; Li, C.; Shi, M.; Zhou, Z.; Huang, C.; Li, F. *Organometallics* **2010**, *29*, 1085.
- (16) Li, J.; Djurovich, P. I.; Alleyne, B. D.; Yousufuddin, M.; Ho, N. N.; Thomas, J. C.; Peters, J. C.; Bau, R.; Thompson, M. E. *Inorg. Chem.* **2005**, *44*, 1713.
- (17) Zamble, D. B.; Lippard, S. J. *Trends Biochem. Sci.* **1995**, *20*, 435.
- (18) DeRosa, M. C.; Crutchley, R. J. *Coord. Chem. Rev.* **2002**, *233*, 351.
- (19) (a) Li, Y.; Tan, C.-P.; Zhang, W.; He, L.; Ji, L.-N.; Mao, Z.-W. *Biomaterials* **2015**, *39*, 95. (b) He, L.; Li, Y.; Tan, C.-P.; Ye, R.-R.; Chen, M.-H.; Cao, J.-J.; Ji, L.-N.; Mao, Z.-W. *Chem. Sci.* **2015**, *6*, 5409.
- (20) Kuznetsova, N. A.; Gretsova, N. S.; Yuzhakova, O. A.; Negrimovskii, V. M.; Kaliya, O. L.; Luk'yanets, E. A. *Russ. J. Gen. Chem.* **2001**, *71*, 36.
- (21) Henderson, L. M.; Chappell, J. B. *Eur. J. Biochem.* **1993**, *217*, 973.
- (22) Grever, C.; Brauer, H. D. *J. Phys. Chem.* **1994**, *98*, 4230.
- (23) Wessels, J. M.; Foote, C. S.; Ford, W. E.; Rodgers, M. A. J. *Photochem. Photobiol.* **1997**, *65*, 96.
- (24) Schweitzer, C.; Schmidt, R. *Chem. Rev.* **2003**, *103*, 1685.
- (25) Yang, E.; Diers, J. R.; Huang, Y. Y.; Hamblin, M. R.; Lindsey, J. S.; Bocian, D. F.; Holten, D. *Photochem. Photobiol.* **2013**, *89*, 605.
- (26) (a) Davies, K. J. A.; Delsignore, M. E. *J. Biol. Chem.* **1987**, *262*, 9908. (b) Wang, W. *Int. J. Pharm.* **2005**, *289*, 1.
- (27) Fancy, D. A.; Kodadek, T. *Proc. Natl. Acad. Sci. U. S. A.* **1999**, *96*, 6020.
- (28) Ghesquière, B.; Jonckheere, V.; Colaert, N.; Van Durme, J.; Timmerman, E.; Goethals, M.; Schymkowitz, J.; Rousseau, F.; Vandekerckhove, J.; Gevaert, K. *Mol. Cell. Proteomics* **2011**, *10*, M110.006866.
- (29) Moan, J.; Berg, K. *Photochem. Photobiol.* **1991**, *53*, 549.
- (30) (a) Li, Y.; Malkaram, S. A.; Zhou, J.; Zempleni, J. *J. Nutr. Biochem.* **2014**, *25*, 475. (b) Liang, X.; Kaya, A.; Zhang, Y.; Le, D. T.; Hua, D.; Gladyshev, V. N. *BMC Biochem.* **2012**, *13*, 21.
- (31) Echevarria, W.; Leite, M. F.; Guerra, M. T.; Zipfel, W. R.; Nathanson, M. H. *Nat. Cell Biol.* **2003**, *5*, 440.
- (32) (a) Tan, K.; Fujimoto, M.; Takii, R.; Takaki, E.; Hayashida, N.; Nakai, A. *Nat. Commun.* **2015**, *6*, 6580. (b) Vives-Bauza, C.; Zhou, C.; Huang, Y.; Cui, M.; de Vries, R. L. A.; Kim, J.; May, J.; Tocilescu, M. A.; Liu, W. C.; Ko, H. S.; Magrane, J.; Moore, D. J.; Dawson, V. L.; Grailhe, R.; Dawson, T. M.; Li, C. J.; Tieu, K.; Przedborski, S. *Proc. Natl. Acad. Sci. U. S. A.* **2010**, *107*, 378.
- (33) Rowland, A. A.; Voeltz, G. K. *Nat. Rev. Mol. Cell Biol.* **2012**, *13*, 607.
- (34) Colombini, M. *Nature* **1979**, *279*, 643.
- (35) Haga, N.; Fujita, N.; Tsuruo, T. *Oncogene* **2003**, *22*, 5579.

(36) Kim, Y. H.; Berry, A. H.; Spencer, D. S.; Stites, W. E. *Protein Eng., Des. Sel.* **2001**, *14*, 343.

(37) (a) Levine, R. L.; Moskovitz, J.; Stadtman, E. R. *IUBMB Life* **2000**, *50*, 301. (b) Winterbourn, C. C.; Hampton, M. B. *Free Radical Biol. Med.* **2008**, *45*, 549.

(38) (a) Kang, B. H. *BMB Rep.* **2012**, *45*, 1. (b) Lee, C.-W.; Park, H.-K.; Jeong, H.; Lim, J.; Lee, A.-J.; Cheon, K. Y.; Kim, C.-S.; Thomas, A. P.; Bae, B.; Kim, N. D.; Kim, S. H.; Suh, P.-G.; Ryu, J.-H.; Kang, B. H. *J. Am. Chem. Soc.* **2015**, *137*, 4358.

(39) Allu, P. K.; Marada, A.; Boggula, Y.; Karri, S.; Krishnamoorthy, T.; Sepuri, N. B. V. *Mol. Biol. Cell* **2015**, *26*, 406.

(40) Reversade, B.; Escande-Beillard, N.; Dimopoulou, A.; Fischer, B.; Chng, S. C.; Li, Y.; Shboul, M.; Tham, P.-Y.; Kayserili, H.; Al-Gazali, L.; Shahwan, M.; Brancati, F.; Lee, H.; O'Connor, B. D.; Schmidt-von Kegler, M.; Merriman, B.; Nelson, S. F.; Masri, A.; Alkazaleh, F.; Guerra, D.; Ferrari, P.; Nanda, A.; Rajab, A.; Markie, D.; Gray, M.; Nelson, J.; Grix, A.; Sommer, A.; Savarirayan, R.; Janecke, A. R.; Steichen, E.; Sillence, D.; Hausser, I.; Budde, B.; Nuernberg, G.; Nuernberg, P.; Seemann, P.; Kunkel, D.; Zambruno, G.; Dallapiccola, B.; Schuelke, M.; Robertson, S.; Hamamy, H.; Wollnik, B.; Van Maldergem, L.; Mundlos, S.; Kornak, U. *Nat. Genet.* **2009**, *41*, 1016.

(41) Suzuki, K.; Kobayashi, A.; Kaneko, S.; Takehira, K.; Yoshihara, T.; Ishida, H.; Shiina, Y.; Oishi, S.; Tobita, S. *Phys. Chem. Chem. Phys.* **2009**, *11*, 9850.

(42) Kwon, T.-H.; Cho, H. S.; Kim, M. K.; Kim, J.-W.; Kim, J.-J.; Lee, K. H.; Park, S. J.; Shin, I.-S.; Kim, H.; Shin, D. M.; Chung, Y. K.; Hong, J.-I. *Organometallics* **2005**, *24*, 1578.